Journal of Molecular Liquids 363 (2022) 119953

Contents lists available at ScienceDirect

Journal of Molecular Liquids

journal homepage: www.elsevier.com/locate/molliq

Ionic liquid solvation of proteins in native and denatured states

Vinicius Piccoli, Leandro Martínez *

Institute of Chemistry and Center for Computing in Engineering & Science, University of Campinas, Campinas, SP, Brazil

ARTICLE INFO

Article history:
Received 14 March 2022
Revised 15 July 2022
Accepted 25 July 2022
Available online 26 July 2022

Keywords:
Molecular dynamics
Solvation
Ionic liquids
Denaturation

ABSTRACT

Ionic liquids (ILs) are utilized as enzymatic reaction solvents and as protein structure protectants or denaturants in biotechnological applications. They can develop a wide spectrum of interactions with macromolecules due to their chemical complexity. Understanding how ILs interact with protein conformations is crucial to fine-tuning their action. Here, we investigate the solvation of different ubiquitin folding states in aqueous solutions of four ionic liquids formed by the combination of the cations 1-Ethyl-3-methylimidazolium (EMIM), and 1-Butyl-3-methylimidazolium (BMIM), and the anions Tetrafluoroborate (BF4), and Dicyanamide (DCA). The structure and thermodynamics of the interactions between the protein in various denaturation states and the ILs were evaluated using minimum-distance distribution functions (MDDFs) and the Kirkwood-Buff (KB) theory of solutions. Under most circumstances, the ILs preferentially solvate the protein structures, and are thus considered denaturants. However, even when preferential hydration is obtained for the native structure, denaturation is favored because of strong IL preferential binding to the denatured states. As the protein undergoes denaturation, its surface area increases, and residues with decreased polarity are exposed. The ILs interact favorably with these residues, excluding water, cooperatively stabilizing the exposure of the protein core. Strong specific DCA-protein interactions, which jointly draw cations to the protein surface due to electrostatic correlations, render ILs containing the anion DCA stronger denaturants than those containing BF4.

1. Introduction

Ionic liquids (ILs) are composed of weakly coordinated ion pairs [1,2]. Due to the poor coordination of the constituent ions, pure ILs are liquid close to room temperatures [3,4]. ILs are important solvents because of their low melting point, low vapor pressure, high polarity, elevated chemical and thermal stability, and low toxicity [5,6]. Their properties can be modified to fit particular applications by carefully selecting cations and anions [5,6]. Biotechnological systems currently comprise an important part of IL applications [7–13], for example as solvents and cosolvents for enzymes and in controlling folding/unfolding reactions [14–19].

In solution, proteins can exist in conformational equilibrium that comprises folded (native) states as well as a variety of partially folded and unfolded forms. In physiological media and ambient circumstances, folded conformations are preferred. By changing the system's thermodynamic state (temperature, pressure, pH), or the solvent composition, the balance between folded and unfolded ensembles can be disrupted [20,21]. According to the most simple mechanism of cosolvent-induced protein denaturation or protection, denaturants interact directly with the protein, whereas protectants are selectively excluded from the protein's proximity [22]. Cosolvents that interact well with the protein favor structures with larger surface area [23–25], frequently denatured states, whereas cosolvents that are preferentially excluded from the protein surface favor more compact protein conformations, which are commonly associated with folded and functional states [26–28]. This model carries, nevertheless, a simplification, which is that the nature of the interactions of the solvent with the exposed solute surface do not change with denaturation. In the context of protein folding, this is similar to assuming that the interactions of the native protein surface with the solution are similar in chemical nature with the interactions of the denatured states. This is not necessarily true, as the residues embedded in the protein core are on average different from the typical solvent-exposed residue. To effectively predict the solvent effect on protein conformational equilibrium, understanding the solvation of the denatured ensembles is necessary [29,30]. From a molecular modeling perspective, studying the denatured ensembles is quite challenging, since these structures are not obtained directly from experimental models. Furthermore, the denatured state is most likely composed of a range of structures of variable compactness, secondary structure preservation, and subdomains.

* Corresponding author at: Institute of Chemistry, University of Campinas, 13083-970 Campinas, SP, Brazil.
E-mail address: lmartine@unicamp.br (L. Martínez).

https://doi.org/10.1016/j.molliq.2022.119953
0167-7322/

Numerous research groups have examined the effect of ions on the structure of water and macromolecular conformations, and ranked the ionic effect on surfaces and interfaces [21,31–34]. The Hofmeister series is a classification system for salt ions based on their propensity to precipitate proteins and macromolecules from aqueous solutions [35,36]. The series classify ions into two distinct groups: those that are highly hydrated and those that are just slightly hydrated [36]. Strongly hydrated ions, such as Fluoride, are classed as kosmotrope ions and have a tendency to preserve the structure of proteins, resulting in salting-out behavior [37,38]. On the other hand, weakly hydrated ions, such as Iodide, favor protein denaturation; these ions are referred to as chaotropes and often exhibit a salting-in action [38–41]. Despite its success in a variety of biological activities, the Hofmeister series exhibits a better predictive ability for anions than for cations [35,42]. The Hofmeister series is, however, imprecise for hydrophobic ILs and lacks a classification scheme for other types of ILs [42,43]. Despite some studies linking hydrophilic ILs to the Hofmeister series effects, [44–46] the interaction between the protein surface and the IL ions is mediated by a complex ionic disruption of hydrogen bonds, non-polar interactions, and electrostatic effects [42,43]. Thus, because the behavior of ILs is strongly influenced by the solvent environment and the type of co-solvent in the system, each IL system should be studied separately to gain a better understanding of how ILs affect protein stability [43,47].

In this work, we aim to advance the comprehension of the denaturing or stabilizing effects of ionic liquids on protein structures by studying the structure and thermodynamics of protein solvation under a range of protein conformations including denatured states. A strategy to sample denatured protein solvation structures is designed, by performing equilibrium simulations of IL-solutions in the presence of static ensembles of proteins with various degrees of denaturation. We explore the interaction of imidazolium ionic liquids with four Ubiquitin conformational ensembles using molecular dynamics, and crucially, minimum-distance distribution functions [48,49], which allow the investigation of the molecular details of highly irregularly-shaped solutes. Kirkwood-Buff integrals and associated preferential solvation parameters allow measurement of the ILs' protective or destabilizing effects associated with each degree of protein conformational denaturation.

2. Methods

2.1. Minimum-distance distribution functions

In this work, we use the *ComplexMixtures.jl* package [49] to compute minimum-distance distribution functions (MDDFs) and associated Kirkwood-Buff integrals and preferential interaction parameters. Detailed formalism associated with these distributions and how they can be used to compute the thermodynamic properties of solutions are described in our previous publications [47,48,50].

In short, MDDFs consist of the distribution of the shortest distance between any solute and solvent atoms. MDDFs are very convenient for the representation of interactions of molecules of complex shapes for automatically taking into consideration the structures of the molecules involved, and thus particularly suited for the study of the solvation of macromolecules with irregular shape. Here, we deal with quaternary solutions composed of a protein (the solute), water, and the IL cation and anion. Because the solution has to be electrically neutral, the distributions of the cation and the anion are correlated, and from a theoretical standpoint, the KB integrals can be computed assuming a pseudo-three component mixture. In other words, the KB integrals of the cation and the anions are equal, something that is expected theoretically [51,52], and confirmed in practice within a range from the protein surface that can be taken into account in simulation studies [47].

The KB integrals can be computed from the counts of minimum-distances between solute (the protein - p) and solvent (water or any other species, c) atoms for each distance r ($n_c(r)$). The cumulative number of sites are obtained in the actual simulated system and in a reference state consisting of a non-interacting mixture with the same species and with the bulk density of the solvent ($n_c^*(r)$),

$$G_{cp} = \frac{1}{\rho_c}\int_0^\infty \left[n_c(r) - n_c^*\right] S(r) dr \tag{1}$$

where $S(r)$ is the surface area element at distance r associated with the minimum-distance from the solute. Eq (1) assumes the most typical radial distribution function when $n_c^*(r) = \rho_c$ and $S(r) = 4\pi r^2$. When the integral of Eq (1) is computed up to a finite distance R, it reduces to

$$G_{cp} = \frac{1}{\rho_c}\left[N_{cp}(R) - N_{cp}^*(R)\right] \tag{2}$$

Where $N_{cp}(R)$ is the number of solute-solvent minimum-distances smaller than R in the solution and $N_{cp}^*(R)$ the MD count in the absence of solute-solvent interactions. $G_{cp}(R)$ converges when R is large enough such that the presence of the solute does not affect the distribution of the solvent molecules, i.e. when $n_c(r) = n_c^*(r)$. The volume defined by the distance to the solute used to proclaim convergence is commonly referred to as the "solute domain", or "protein domain" in the present work. Therefore, the KB integrals are computed from the fluctuations in the number of solvent molecules within the protein domain, which is an open system embedded in a larger solvent reservoir. The concentration of the reservoir is computed from the simulation, correcting the bulk solvent densities from variations associated with the accumulation or depletion of the solvent molecules from the protein domain. Both these strategies were suggested by Ganguly and co-workers [53] to improve the convergence of KB integrals relative to the explicit integration of the distribution function. Despite these methods, KB integrals, particularly for the extended systems, exhibit some convergence problems, particularly with BMIM and DCA because of the size and protein affinity of the ions, as depicted in Figures Supplementary Figs. S4, S8, S12, and S16.

Preferential solvation parameters are computed from the difference between KB integrals of the components of the solvent using

$$\Gamma_{cp}(R) \approx \rho_c\left[G_{cp}(R) - G_{wp}(R)\right] \tag{3}$$

where the subscripts cp and wp refer to IL-protein and water-protein [54–57]. If $\Gamma_{cp}(R)$ is positive (the KB integral of the IL is greater than that of water), the protein is preferentially solvated by the IL.

2.2. Stabilizing and denaturing cosolvents

The preferential solvation parameter can be used to study a cosolvent's denaturant or protectant effect on the macromolecular structure. For example, if $\Gamma_{cp}(R)$ is positive, solvent c interacts favorably with the protein surface and stabilizes structures with a larger surface area, which are most often associated with denatured states [21,58–62]. On the other hand, if the protein is preferentially hydrated, the cosolvent is excluded from the protein surface, favoring more compact structures, usually associated with folded and functional protein conformations. This is the reasoning for osmolytes' overall stabilizing or destabilizing effects on protein structures, which assumes that the chemical composition of the protein surface does not change considerably during denaturation

[27,58,63]. This assumption is of course only partially valid for proteins, which typically display different compositions of amino acids exposed to the solvent and in their hydrophobic cores. The chemical nature of the protein surface thus changes with denaturation, in such a way that it is not safe to deduce the denaturing or stabilizing effect of an osmolyte from its interactions with the native protein state alone [24,64].

2.3. Protein conformations

We study the solvation of Ubiquitin in 4 folding states: the *native*, *perturbed*, *denatured*, and *extended* states. For each of these states, 20 independent structures were used as initial configurations for equilibrium MD simulation in various solvents. The construction of these structure sets is described below.

The *native* set corresponds to the crystallographic structure (PDB code: 1UBQ [65]) following standard equilibrium simulation protocols, which are described in the next section. These structures differ from the crystallographic model by 1.76 Å RMSD and preserve 95 % of the crystallographic contacts, as shown in Table 1. The VMD software was used to identify the residues in the protein core of the native structure using the "buried" selection attribute. It is composed of the amino acids methionine (1 residue), isoleucine (8 residues), phenylamine (2 residues), valine (5 residues), leucine (9 residues), and alanine (2 residues). Thus, the hydrophobic core of Ubiquitin is formed exclusively by hydrophobic residues, and the denaturation of the structure will expose this largely apolar surface to the solvent.

The *perturbed* set was obtained by performing short (50 ns) simulations of the structure solvated by water at 500 K. These simulations resulted in a set of conformations with an average RMSD relative to the crystallographic structure of 3.6 Å and preserved 75 % of the crystallographic contacts. Thus, these are partially denatured protein states, which preserve globularity and most of the native secondary and tertiary structures.

The *denatured* set was obtained by performing a single longer (100 ns) simulation of the protein structure in a vacuum at 600 K. Equally spaced frames from this simulation were extracted at every 5 ns, and used as initial conformations for MD simulations. These conformations diverged from the crystallographic structure by 12 Å RMSD and preserve 37 % of the crystallographic contacts. Therefore, these are significantly denatured structures which expose the hydrophobic core of the protein.

Finally, the *extended* set was constructed to represent the upper limit of possible protein solvent surface exposure and denaturation. It was constructed as a linear, extended, chain of amino acids of UBQ with dihedral angles $\varphi = 180^{\circ}$ and $\psi = 180^{\circ}$. The conformation was constructed with the *Molefacture* VMD plugin. To achieve such a conformation, 3 Proline residues were mutated to Alanines. Table 1 summarizes the main structural properties for the conformations used.

For each of these folding states, 20 structures were obtained, which were independently used for equilibrium molecular dynamics simulations in an explicit solvent of variable compositions, as described in the next section.

Fig. 1 illustrates representative structures of native, perturbed, denatured, and extended ensembles. The native ensemble retains the majority of the crystallographic structure's structural properties (Fig. 1A), whereas the perturbed structure loses some secondary structure (Fig. 1B). The denatured structures (Fig. 1C) have lost almost all of their secondary structures and have a globular shape that is variable. Fig. 1D illustrates the extended structure. This conformation is used to simulate an extreme state of denaturation, without any structural resemblance to the other ensembles (red structure in Fig. 1D).

2.4. Molecular dynamics simulations

Equilibrium molecular dynamics simulations of the structures solvated by water and a variety of IL pairs and concentrations were performed using GROMACS.2018.3 CUDA [66,67]. The initial configurations of the systems were built with Packmol [68,69]. Parameters to describe the ionic liquids and the protein were obtained, respectively, from the virtual-site OPLS [70], and OPLS-AA force fields [71], and the water model used was the TIP3P model [72]. Numerical integration of the equations of motion was performed using the Verlet leapfrog algorithm with a timestep of 2 fs. A cutoff of 1.0 nm was used for short-range electrostatic and Lennard-jones interactions. The long-range electrostatics were calculated using particle-mesh Ewald [73] summation with a fourth-order interpolation and a grid spacing of 0.16 nm. The temperature of the systems was set to 300 K. The modified Berendsen thermostat was used to keep the temperature fixed with a relaxation time of 0.1 ps [74,75].

Using the Parrinello-Rahman algorithm with a relaxation time of 2 ps and isothermal compressibility of 4.5 10^{-5} bar, the pressure was kept constant at 1 bar [76,77]. Each system's energy was originally minimized for 50,000 Steepest-Descent [78] steps while all protein coordinates remained constant. 1 ns of thermal equilibration in the NVT ensemble was followed by 5 ns MD in isothermic-isobaric (NPT) conditions with the protein backbone fixed. The restrictions employed in simulations with the native conformation were removed after these stages, and 1 ns simulations with constant pressure and temperature were undertaken. Production simulations lasted 10 ns and were run in the NPT ensemble as well. Each structure set consisted of 20 conformations that were simulated separately using the procedure outlined above. We chose to run many brief simulations since the Ubiquitin structure stays closer to the initial state, and we get a good sample of the solvent structure. Soft harmonic constraints with a 10 kJ mol^{-1} $Å^{-2}$ force constant were added to the Cα atoms of the structures, preventing the structures from rotating. This allowed the use of simulation boxes with dimensions adjusted for each conformation. These constraints were not required in the simulations of the folded state because a cubic box was used.

As described above, the folded and unfolded states do not represent the structures that would be obtained in equilibrium simulations of Ubiquitin in these solvents (which would require very long and accelerated sampling simulations for each solvent condition). Thus, the present simulations address the effect of the presence of the ILs in the thermodynamic states of the protein in

Table 1
Average and standard deviation of the solvent-accessible surface area (SASA), gyration radii, RMSD relative to the crystallographic model, and the fraction of native contacts - NC (Cα distances shorter than 7 Å) for all conformation sets. The conformations of the extended set have identical backbone coordinates, and thus the deviations do not apply.

Structure set	SASA (10^2 $Å^2$)	Gyration radius (nm)	RMSD (Å)	NC
Native	49.70 ± 0.05	1.179 ± 0.002	1.76 ± 0.02	0.95 ± 0.01
Perturbed	53.0 ± 0.4	1.221 ± 0.008	3.6 ± 0.02	0.75 ± 0.03
Denatured	74 ± 9	1.292 ± 0.007	12.15 ± 0.06	0.37 ± 0.01
Extended	117.4	8.01	76.7	0

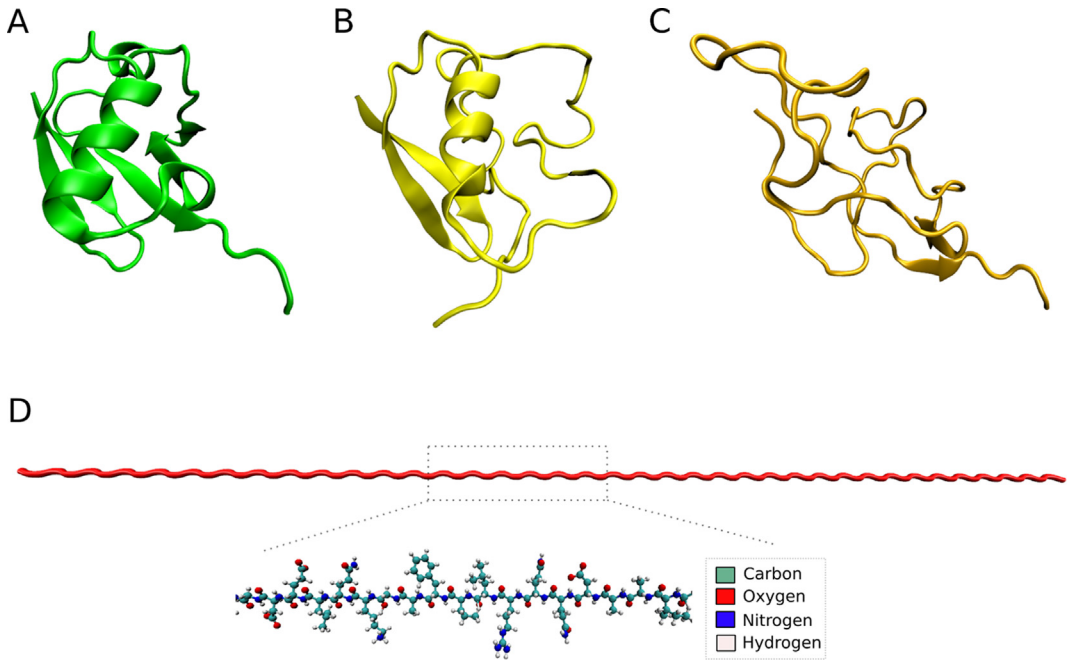

Fig. 1. Representative models of A) native, B) perturbed, C) denatured, and D) extended structures. From native to the denatured state, the structures lost their secondary structures, assuming a globular shape with exposed core residues.

folding states that may be induced by extraneous agents, such as temperature and pressure variations, and capture essentially the role of the exposure of the protein core to the solvent.

The MDDFs, KB integrals, and discrimination of solute and solvent atomic contributions are computed using the ComplexMixtures.jl [49,79] package. The density was derived from the average number of minimum-distances at each 0.1 Å bin, and the minimum-distance distribution functions were constructed using a discretized version of Eq. (1). Eqs (2) and (3) were used to get the KB integrals and preferential solvation parameters. To declare KB integral convergence, we choose R = 20 Å in all systems (which is unusually large [48,80], demands large solvation boxes, and was required because of the size and electrostatic nature of the IL ions). The solution volume closer to the solute than this distance was therefore considered the "protein domain", i. e. the region of the solution where the solution structure is affected by the presence of the protein. The volume outside this domain contains the mixture of cosolvents and is used to deduce the structure and thermodynamic properties of the solution without the protein (for instance, the effective bulk concentration of the solutions is obtained from this region of the simulation box).

The ionic liquids (ILs) used are a combination of the cations EMIM (1-ethyl-3-methylimidazolium) and BMIM (1-butyl-3-methylimidazolium) and the anions DCA (dicyanamide) and BF4 (butyl-3-methylimidazolium) (tetrafluoroborate). 0.5, 1.0, 1.5, 2.0, 2.5, and 3.0 mol/L EMIMDCA, EMIMBF4, BMIMDCA, and BMIMBF4 solution concentrations were simulated. Table 2 shows the data for the systems with EMIMDCA and the various structure sets that were used. Supplementary Tables S2 and S3 provide details on the remaining systems. Using the bulk region of the simulation box, the concentrations of each system were recalculated from the NPT production.

It is important to mention that Ubiquitin does not have a net charge, permitting the simulation to contain only the protein, water, and the ions of the ionic liquids. Since the only ions in the solution are those of the ILs, charge neutrality implies that they can be considered equivalent species in the computation of KB integrals, and the system can be treated as a pseudo-three component mixture. This simplifies the use of KB theory significantly relative to systems where the solute is not neutral or multiple ionic species are present [18,59,81].

The data presented in this work are averages of the 20 simulations performed for each system, with the standard error of the mean of these replicates displayed where relevant. Hydrogen-bonds were calculated using VMD [82] with default geometrical settings, with the Fluorine atoms of BF4 serving as probable H-bond acceptors.

The complete sets of distribution functions, KB integrals, and preferential interaction parameters are available as Supplementary Figures. These include the MDDFs displayed at greater distances than those in the paper figures, and the proper visualization of the quality of the convergence of all quantities computed.

3. Results and discussion

3.1. Preferential solvation and protein stability

ILs' preferential solvation parameters can be used to summarize the solvation of various protein conformation sets [83]. This information is essential for comprehending the role of the solvent in denaturation and protection of protein conformations [27,83]. The IL solutions were simulated with four different structure sets: native, perturbed, denatured, and extended. Fig. 2 shows preferential solvation parameters (Γ_{cp}) obtained. For practically all systems, the outcome the Γ_{cp} increases from 0.5 to 1.5 mol/L, then falls from 1.5 mol/L onwards. Γ_{cp} greater than 0 denotes that the cosolvents (ionic liquids) preferentially solvate the protein. Notable exceptions are a few native structures at higher IL concentrations: in B, C, and D the native structures display negative IL solvation parameters at the greater concentrations, indicating that the protein is preferentially hydrated.

The IL-protein preferential solvation parameter, Γ_{cp}, for various EMIMDCA concentrations are shown in Fig. 2A. The typical behavior of Γ_{cp} as a function of IL concentration in all structure sets (native, perturbed, denatured, and extended) is that of an initial increase that reaches a maximum value and then drops in more

Table 2
Simulation boxes used and concentrations for water and ions after the NPT equilibration for EMIMDCA systems. Fluctuations were calculated using the standard error of the mean calculated for each concentration's 20 simulations. The corresponding data for the other IL solutions are shown in Supplementary Tables S2 and S3.

Ionic liquid / Conformation	RC	Box sides (Å)	Number of molecules		Concentration (mol/L)		%wt
			ions	water	water	ions	
EMIMDCA (NATIVE)	0.5	95.1	254	25,761	50.73 ± 0.02	0.46 ± 0.02	8.46
	1.0	95.1	507	23,292	46.53 ± 0.03	0.96 ± 0.04	17.65
	1.5	95.1	760	20,824	42.0 ± 0.1	1.49 ± 0.05	26.43
	2.0	95.1	1014	18,357	37.49 ± 0.05	2.03 ± 0.01	35.23
	2.5	95.1	1269	15,888	32.59 ± 0.05	2.6 ± 0.01	44.02
	3.0	95.1	1522	13,420	27.86 ± 0.03	3.15 ± 0.01	52.75
EMIMDCA (Perturbed)	0.5	93.0	239	24,248	50.63 ± 0.02	0.46 ± 0.03	8.8
	1.0	93.0	479	21,885	46.45 ± 0.04	0.94 ± 0.01	17.7
	1.5	93.0	718	19,532	41.96 ± 0.04	1.47 ± 0.05	26.6
	2.0	93.0	958	17,170	37.24 ± 0.05	2.02 ± 0.05	35.4
	2.5	93.0	1197	14,817	32.39 ± 0.04	2.58 ± 0.05	44.3
	3.0	93.0	1436	12,464	27.47 ± 0.04	3.15 ± 0.01	53.1
EMIMDCA (Denatured)	0.5	84.9, 92.5, 130.5	244	24,781	50.8 ± 0.02	0.44 ± 0.03	8.83
	1.0	84.6, 92.2, 129.4	489	22,396	46.69 ± 0.05	0.93 ± 0.05	17.6
	1.5	84.3, 91.9, 129.6	733	20,021	42.25 ± 0.05	1.44 ± 0.05	26.4
	2.0	84.0, 91.5, 129.1	978	17,636	37.67 ± 0.06	1.97 ± 0.07	35.3
	2.5	83.7, 91.2, 128.7	1222	15,261	32.77 ± 0.05	2.54 ± 0.05	44.0
	3.0	83.8, 91.3, 128.2	1466	12,886	27.93 ± 0.03	3.11 ± 0.05	52.8
EMIMDCA (Extended)	0.5	68.4, 74.3, 333.6	504	51,165	50.78 ± 0.03	0.45 ± 0.04	8.84
	1.0	68.1, 74.1, 332.4	1009	46,277	46.69 ± 0.05	0.93 ± 0.01	17.6
	1.5	67.9, 73.8, 331.2	1513	41,399	42.41 ± 0.04	1.44 ± 0.04	26.4
	2.0	67.7, 73.6, 330.0	2018	36,511	37.7 ± 0.04	1.99 ± 0.05	35.2
	2.5	67.5, 73.3, 329.0	2522	31,633	32.95 ± 0.05	2.54 ± 0.01	43.9
	3.0	67.2, 73.0, 327.7	3026	26,755	28.05 ± 0.03	3.12 ± 0.04	52.6

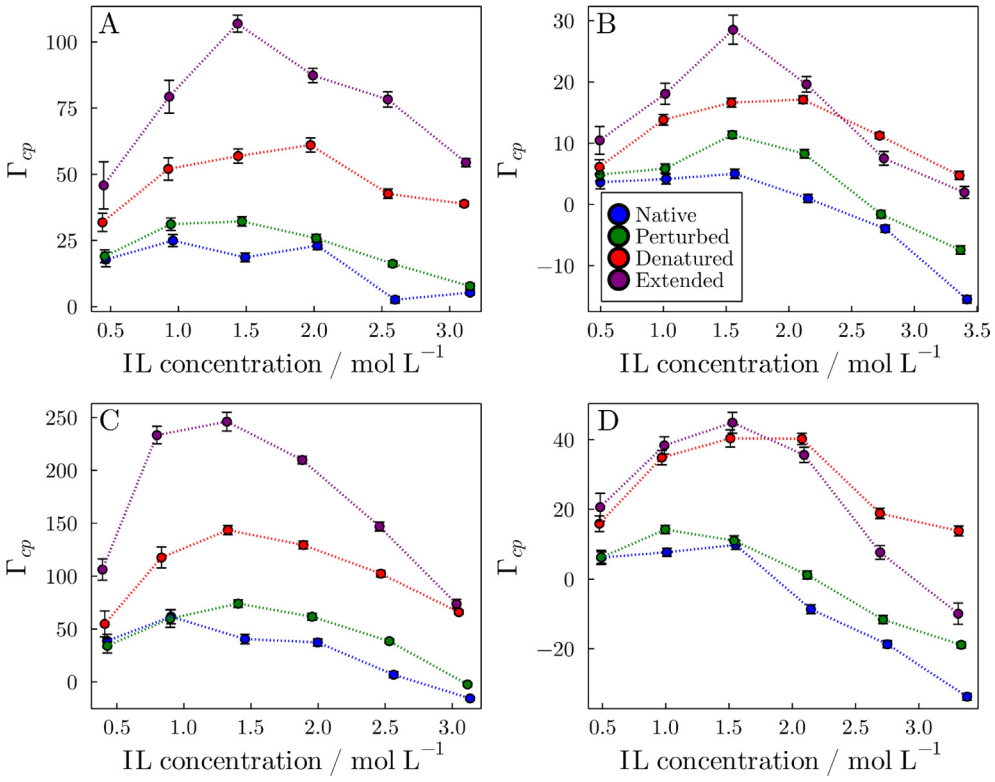

Fig. 2. Preferential solvation coefficients (Γ_{cp}) for the Ionic Liquids A) EMIMDCA, B) EMIMBF4, C) BMIMDCA, and D) BMIMBF4 in systems with native, perturbed, denatured, and extended conformations sets. The concentrations displayed in the x-axis are the bulk IL concentrations recalculated after the system simulations. Table S8 in the Supplementary material contains the raw preferential solvation and preferential hydration parameters.

concentrated systems. For example, the curve for extended structure systems (purple curve in Fig. 2A) reveals that Γ_{cp} increases from 0.5 to 1.5 mol/L to about ~107. Then, Γ_{cp} drops as the concentration increases from 1.5 mol/L onwards, to ~54 for the system with the maximum IL concentration.

Fig. 3 shows an example of all BMIMBF4 concentrations with native and perturbed folding states utilizing all BMIMBF4 concentrations. BMIM first solvation shell number (FSSN) of molecules is greater around the perturbed ensembles, as seen in Fig. 3A. The water FSSN of the perturbed ensemble is smaller than that of the

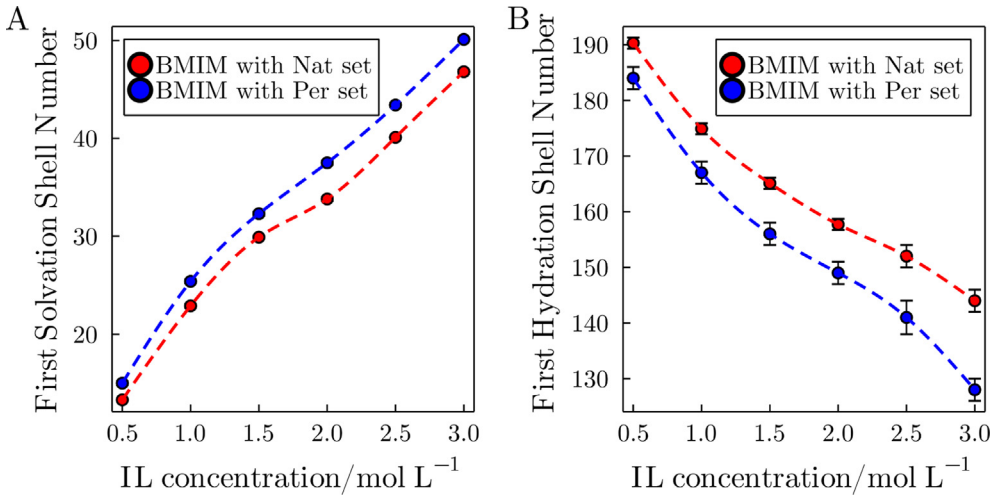

Fig. 3. First solvation shell numbers (FSSN) of BMIM in the presence of BF4 for native and perturbed protein ensembles. A) First solvation shell number of BMIM cation up to 3.8 Å. B) First hydration shell number of water molecules up to 2.5 Å. Similar data for other systems is available in Supplementary Table S7.

native ensemble in all concentrations, even if the surface area of the perturbed set is greater than that of the native state (Fig. 3B). This means that the exposure of residues of the hydrophobic core promote the accumulation of IL cation on the surface in such a way to expel water molecules from the vicinity of even the residues which were hydrated in the native structure.

Overall, the interaction of the ionic liquid with the protein becomes favorable for configurations with greater unfolding degree. The saturation of the stronger interaction sites for the IL on the protein surface occurs for all structure sets, but is enough to lead to preferential hydration only for the extended protein in solutions with 3.0 mol/L of EMIMBF4, BMIMDCA, and BMIMBF4. The molecular basis for ILs preferentially solvation of unfolded structures will be described in the next section, but one important feature that must be mentioned here is the thermodynamic implications of the greater Γ_{cp} observed in denatured states relative to the native state.

In Fig. 2, we have seen that Γ_{cp} increases with the unfolding of the structures for most of the simulated systems. Eq (4) connects the equilibrium constant of a putative two-state folding equilibrium to the difference in the preferential solvation coefficients of the cosolvent with the protein in two different folding states:

$$\left(\frac{\partial \ln K}{\partial \ln a_3}\right)_{m2} = \Delta\Gamma = \Gamma_{unfolded} - \Gamma_{folded} \tag{4}$$

where K is the equilibrium constant for the folding reaction *Folded* $\leftrightharpoons$ *Unfolded*, and a_3 is the activity of the cosolvent [27,83,84].

If the difference, for instance, between Γ_{cp} for native and denatured conformation sets is positive ($\Gamma_{cp}(denatured) - \Gamma_{cp}(native) > 0$), the equilibrium constant increases with the increase in the activity of the cosolvent, thus the denatured state will be favored. Thus, $\Delta\Gamma_{cp}$ can be directly connected to the displacement of the equilibrium this hypothetical folding equilibrium with the addition of a cosolvent. $\Delta\Gamma_{cp} > 0$ implies that increasing the cosolvent concentration favors denatured over native structures. On the other hand, if $\Delta\Gamma_{cp} < 0$, the native state is favored by the increase in the concentration of the cosolvent. As a result, cosolvents with $\Delta\Gamma_{cp} < 0$ can be classified as protectants, while those with $\Delta\Gamma_{cp} > 0$ can be classified as denaturants.

The difference in Γ_{cp} between each denatured state and the native states is shown in Fig. 4 as a function of IL concentration. Essentially, we have $\Delta\Gamma_{cp} > 0$ for all systems at all concentrations (except for the lower concentrations of BMIMDCA in Fig. 4C, where it is close to zero). Therefore, the ILs will displace the folding equilibrium towards denatured states. This is the case even for the systems in which the native protein is preferentially hydrated, which would suggest a protecting role for the cosolvent. For example, the Γ_{cp} for the system with the native structure of Ubiquitin, as in the system with 3.0 mol/L of BMIMBF4 is negative. As a result, the IL appears to have a protective effect on the protein structure, as it is preferentially excluded from the protein's domains. However, IL Γ_{cp} for the denatured systems at 3.0 mol/L BMIMBF4 is greater than that of the native state. In this case, the result would be $\Delta\Gamma_{cp} > 0$, implying that the solvent favors the unfolded structures.

In general, the more advanced the denaturation state of the protein, the greater the $\Delta\Gamma_{cp}$ relative to the native structure, for a given concentration. As a result, there is a cooperative relationship between the protein's denaturation and its interactions with the IL. As the protein denatures, the chemical nature of the protein surface becomes increasingly affine to the IL, favoring additional protein surface exposure.

In summary, the ILs simulated preferentially solvate Ubiquitin. This preferred solvation is more successful for sets of denatured and extended structures. BMIMDCA and BMIMBF4 stood out in particular by having the highest and lowest preferential solvation parameters, respectively. These findings are in agreement with previous studies that also investigated the effect of ionic liquids on protein structures. [85–87].

3.2. Solvation structure of systems with 1.5 mol/L EMIMDCA and EMIMBF4

In this section, we focus on individual systems to understand the molecular basis of the protein-IL ion interaction. Minimum-distance distribution functions and KB integrals will be used to analyze systems containing 1.5 mol/L solutions of the ionic liquids EMIMDCA, EMIMBF4, BMIMDCA, and BMIMBF4. These distribution functions and KB integrals were used for the computation of the preferential interaction parameters discussed in the previous sections. Similar conclusions can be drawn from the other concentrations, all corresponding data being available in the Supplementary Information.

Fig. 5A and 5B show, respectively, MDDFs and KB integrals of DCA in systems with ~1.5 mol/L EMIMDCA solutions relative to each Ubiquitin structure set. There is a distinct peak at ~1.9 Å, associated with hydrogen bonds. At this distance, the DCA density is up to 5 times greater than in the reference condition, for the native state (blue curve in Fig. 5A). The peak becomes less pronounced

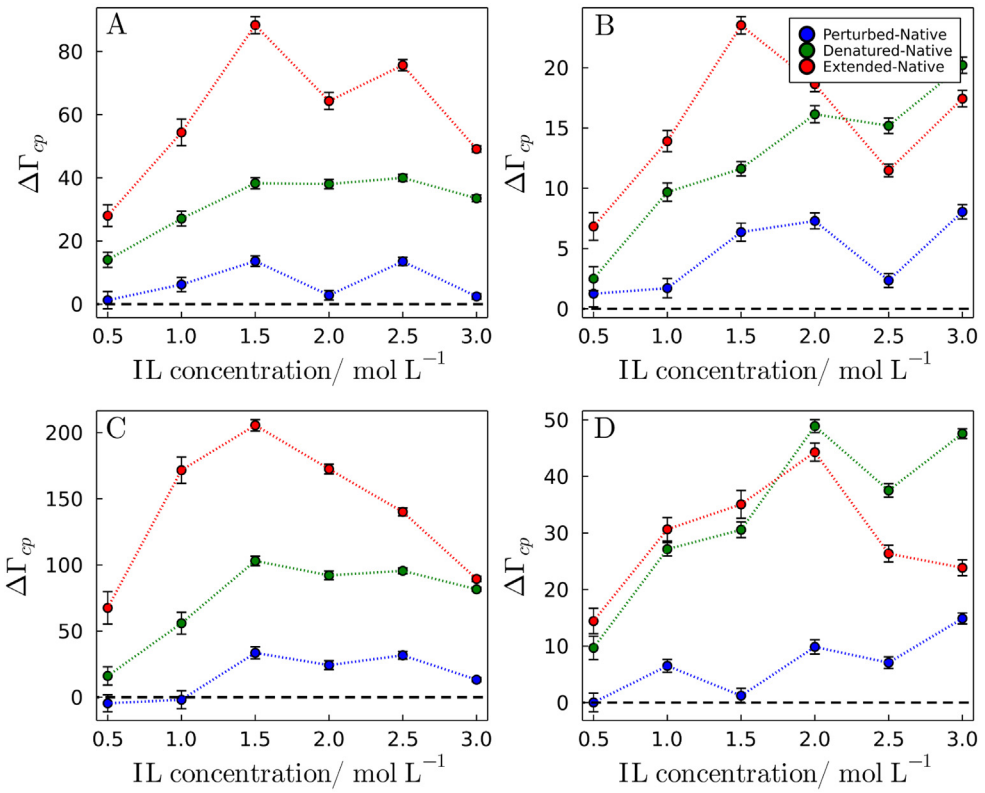

Fig. 4. Variation of the IL preferential solvation coefficients ($\Delta\Gamma_{cp}$) for the Ionic Liquids A) EMIMDCA, B) EMIMBF4, C) BMIMDCA, and D) BMIMBF4. Red, green, and blue curves are, respectively, the difference of Γ_{cp} in systems with extended/native, denatured/native, and perturbed/native conformations. Here, the concentrations displayed are the reference concentration, which are the ones used to build the initial system. The black dashed line indicates $\Delta\Gamma_{cp} = 0$. (For interpretation of the references to color in this figure legend, the reader is referred to the web version of this article.)

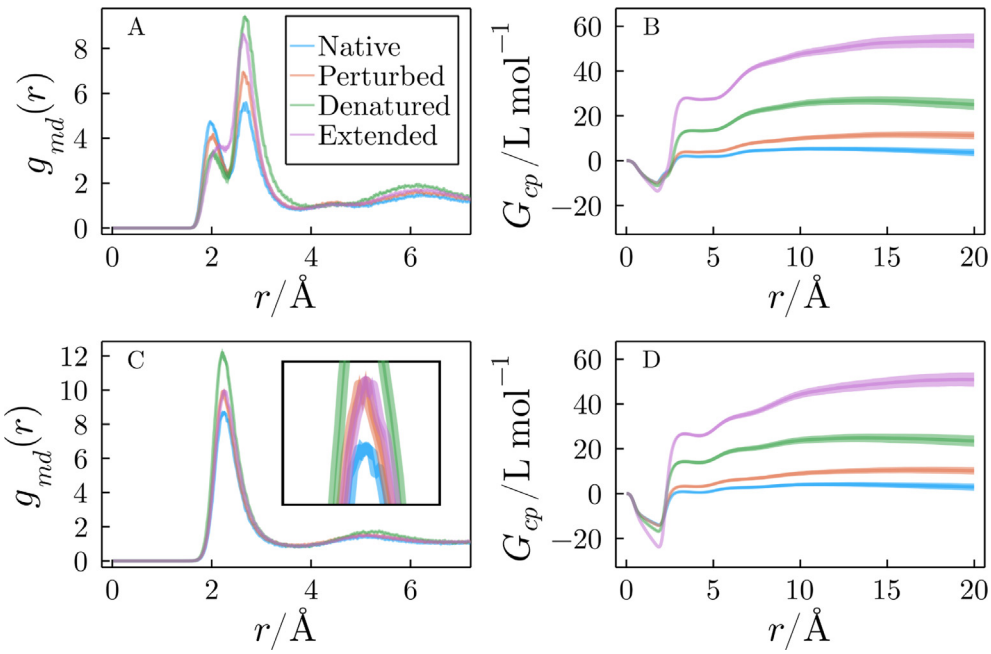

Fig. 5. (A) MDDFs and (B) KB integrals for DCA relative to Ubiquitin in different conformational states in solutions of ~1.5 mol/L EMIMDCA. (C) MDDFs and (D) KB integrals for EMIM in the same solution. In (A), we observe that DCA local density augmentation at hydrogen-bonding distances decreases as the protein undergoes denaturation, while the local density at non-specific (interactions different from hydrogen bonds) interactions increase. In (C), the EMIM MDDFs display higher peaks with unfolded protein states; the extended MDDF curve (Purple) overlaps almost exactly with the Perturbed MDDF (orange), as displayed in the inset (C). (B) and (D), respectively, depict DCA and EMIM KB integrals, which are similar because of electrostatic correlation, and become greater as the structure of the protein becomes increasingly unfolded. (For interpretation of the references to color in this figure legend, the reader is referred to the web version of this article.)

as the protein undergoes unfolding. For the perturbed, denatured, and extended conformations, the MDDF peak corresponding to hydrogen-bonding has maximum values of ∼4.1, ∼3.8, and ∼3.6, respectively. The peak at ∼2.5 Å, on the other hand, is associated with non-specific interactions [18], and exhibits nearly an inverted trend: the DCA density is higher in sets with structures of greater surface area. Thus, the MDDFs support a predictable trend of interactions: polar interactions are relatively more important for the folded state of the protein and non-specific, hydrophobic, interactions are magnified with the exposure of the protein core.

Fig. 5B shows KB integrals for the DCA anion. At short distances, $r < 1.5$ Å, there is a drop in all KB integrals that is due to the protein excluded volume. The first drop is followed by an accumulation step that involves specific and non-specific direct interactions, at the 1.9–5.0 Å range (Fig. 5A). The diffuse peak of the MDDF at ∼6 Å also contributes significantly to the final KB integral. The converged KB integrals indicate a DCA accumulation in the protein domain that follows the increase of the structure surface area. For example, the DCA KB integral relative to the native structure set (blue curve) is negative, indicating that the accumulation at long distances was insufficient to compensate for the initial exclusion. The DCA KB integrals for the other structural sets, on the other hand, are positive, indicating that DCA has a greater concentration on the protein domain than in bulk.

Fig. 5C shows that EMIM MDDFs contain only one peak, at ∼2.4 Å. This peak is related to non-specific interactions between protein structures and EMIM cations. The MDDF peaks indicate how favorable the interactions are (between solvent and solute) [16]. The EMIM MDDF peak is smaller in the extended conformation than in systems with denatured structures. Besides that, as can be shown in Fig. 5C, the MDDFs in the perturbed and extended systems are overlapped. Thus, the interactions between the cations and extended conformations are less favorable than in denatured conformations and comparable with perturbed conformations.

Fig. 5B and 5D show that the KB integrals are greater for the extended conformation set. This happens because of its greater surface area (Eq. (1)). This effect can be seen by comparing MDDFs and KB integrals in systems with native and extended structure sets (blue and purple curves, respectively). Although the IL MDDFs of the perturbed and extended sets are similar, the KB integral calculated using the MDDF in the system with extended conformations is more than 3 times greater than the KB integrals relative to native structures. In summary, the interaction between each IL ion and the extended conformation surface is less favorable on average (as shown in Figs. S2 to S17), but the overall ion accumulation is greater in the protein domain because there is a greater protein surface area exposed (as shown in Figs. 1 and 3).

It is also important to note that the KB integrals of DCA (Fig. 5B) and EMIM (Fig. 5D) are similar. This is because the anion and cations cannot have different long-range concentration differences, which would imply breaking the local electroneutrality of the solution (in KB theory this is referred to as the equivalence principle). For the bulk solution to remain electrically neutral, the KB integral, which measures the effective accumulation of species around the protein, must converge to the same value for cations and anions. This indicates that the number of excess cations and anions in the protein domain are equal. This cooperative effect has been examined in greater depth in a previous publication [47].

The MDDFs are broken down into contributions of classes of amino acid residues in Fig. 6. The contribution of polar and basic

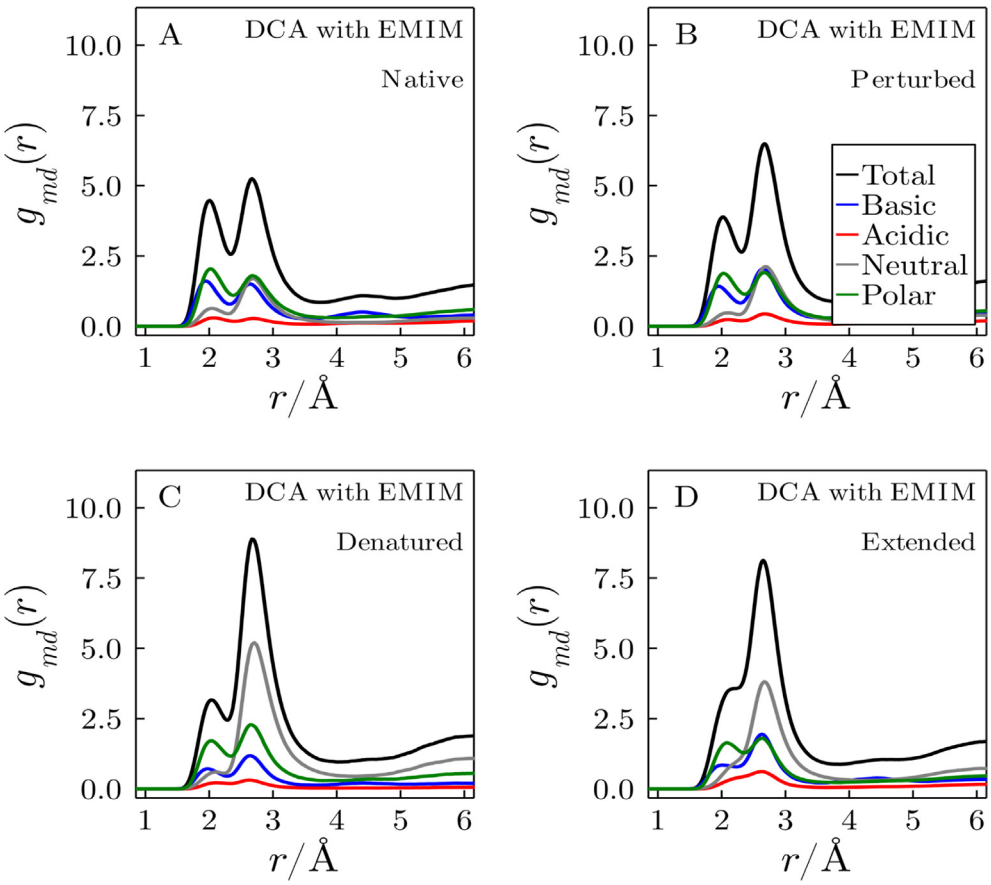

Fig. 6. Effect of folding state in the distribution functions of the DCA: discerning the contributions of each residue type, at an IL concentration of ∼1.5 mol/L. A), B), C), and D) are, respectively, DCA distributions with native, perturbed, denatured, and extended structures set. The first peak, at ∼1.9 Å, indicates greater accumulation on polar and basic residues, while the peak at ∼2.7 Å is associated with DCA accumulation on neutral residues.

residues to the hydrogen bond peak (at 1.9 Å) is significant. The second peak (at 2.6 Å) also has contributions from polar and basic residues, but neutral (mainly aliphatic) residues also answer for an important part of the interactions. Since the peak of hydrogen bonds falls as the degree of unfolding grows, whereas the peak of nonspecific interactions increases, the contribution of neutral residues to total MDDF increases considerably upon denaturation.

The contribution of the protein amino acid classes to the cation MDDF is depicted in Fig. 7. Polar and neutral residues contribute the most to the MDDFs of the native conformations. The contribution of neutral (aliphatic) residues becomes more important as the protein structure undergoes unfolding. The structures with greater surface area exposed to the solvent make its aliphatic residues available to possible non-specific interactions with EMIM ions. This can be identified by the increasing of the neutral residue's contribution to the total cation MDDF from Fig. 7A to Fig. 7D.

The MDDFs (Fig. 5A and 5C) have already demonstrated that the ions interact with the protein differently. Fig. 8 shows the map of ions around each protein residue. The DCA density is greater than EMIM in orange regions, while the EMIM density is lower in blue regions. Orange regions at 1.9 Å can be linked to the first peak of DCA MDDF (at 1.9 Å in Fig. 5A), especially with the following residues: M1, K6, *K*11, Q31, R42, K48, Q49, and R74, which are mostly polar and positively charged. Negatively charged and hydrophobic residues such as I3, T7, L8, D32, I44, and L73 contribute primarily to regions where EMIM concentration is higher than DCA (blue regions). It is worth noting that the figure occasionally depicts regions with higher DCA concentrations around negative residues, such as E16. Because the residues in Fig. 8 are near to one another, this results from representation's deception rather than the system's actual interactions.

The difference in ion density for the ensemble of denatured structures is shown in Fig. 8B. The main qualitative difference is the increase in densities at 2.4 and 2.7 Å, followed by a reduction in the relative accumulation of ions at 1.9 Å. It's worth noting that the concentrations of both DCA and EMIM rise sharply around the apolar residues. When compared to the native ensemble map, there is a large EMIM density increase around residues I3, F4, L8, I13, L43, I44, L50, L56, I61, L69, V70, L71. This indicates that ions, particularly the cations, interact strongly with hydrophobic residues from more unfolded structures. The anion (DCA) accompanies the cation, leading to the rise in the increased DCA concentrations at ~2.6 Å. This provides an interesting rationale for a cooperative mechanism of protein denaturation by IL: the hydrophobic nature of the cation allows the solvation of the residues that are exposed upon denaturation. This would increase the local positive charge of the surface, which could become rapidly saturated. However, the anion is strongly correlated with the cation and neutralizes this local anion accumulation. This leads to almost complete coverage of the exposed surface by the IL, favoring strongly denatured protein states.

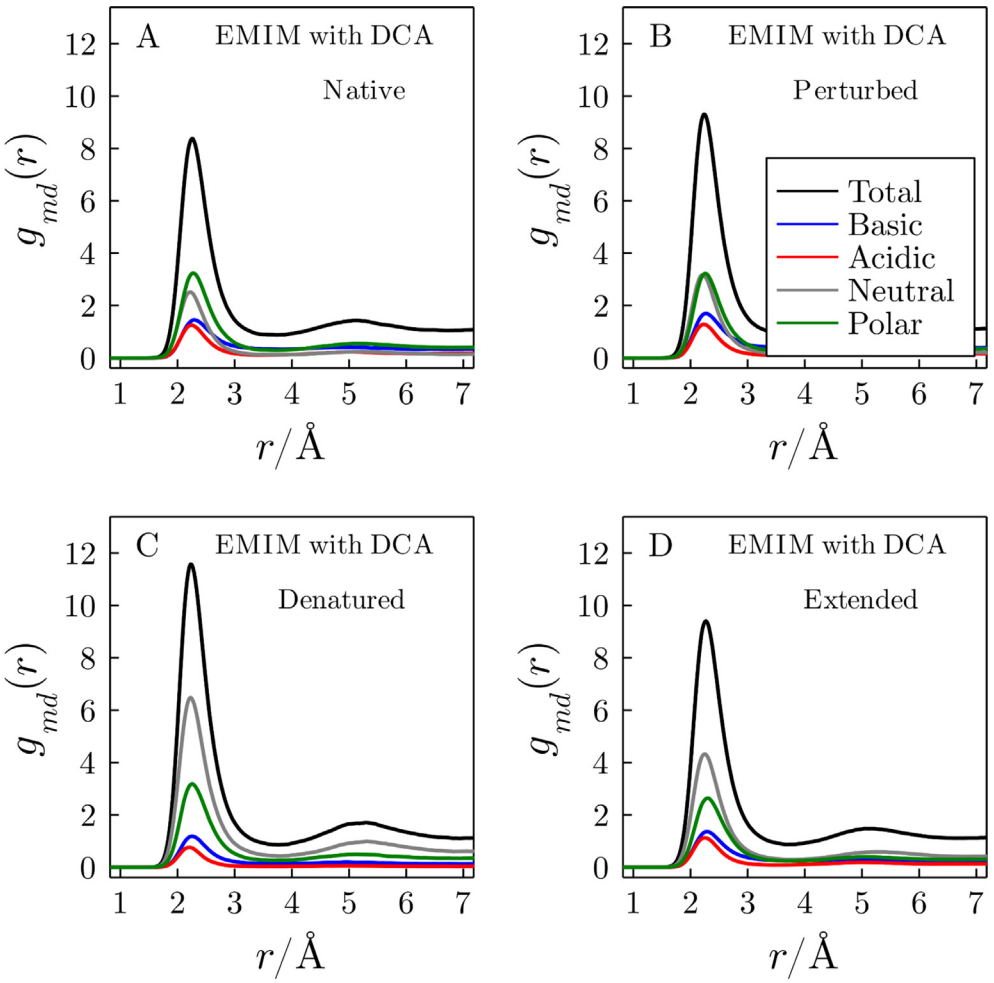

Fig. 7. Effect of the folding state in the distribution functions of the DCA: discerning the contributions of each residue type, at an IL concentration of ~1.5 mol/L. A), B), C), and D) are, respectively, EMIM distributions with native, perturbed, denatured, and extended structures set. The peak, at ~2.4 Å, indicates a greater accumulation on neutral residues with the progressive unfolding.

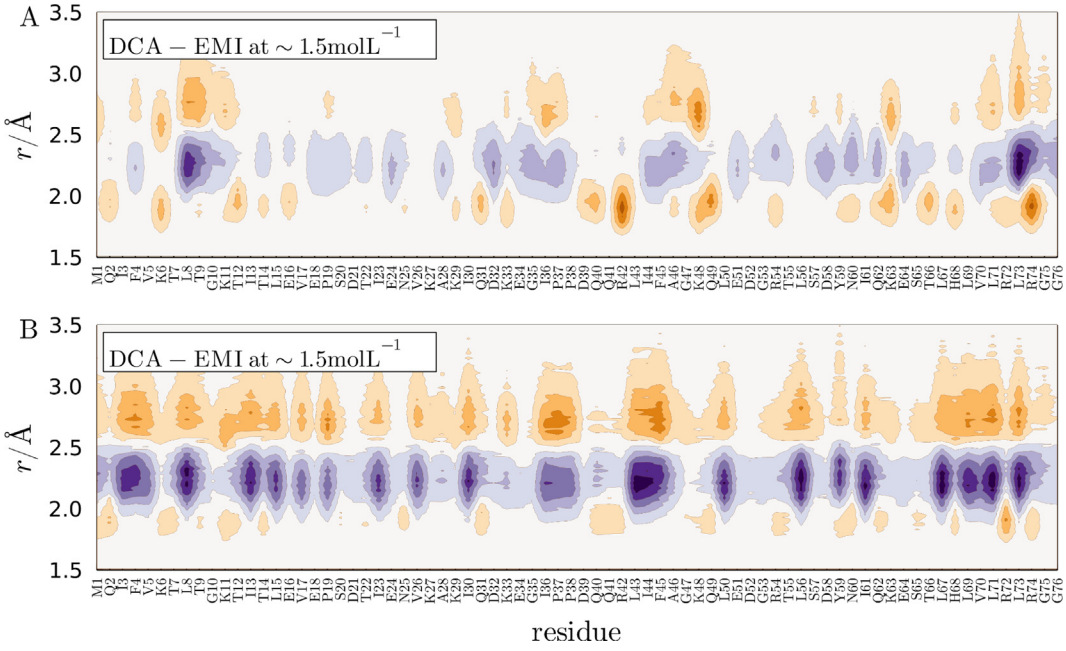

Fig. 8. Difference in densities of the ions in the vicinity of the native (A) and denatured (B) protein conformations at ∼1.5 mol/L of EMIMDCA. The blue color represents regions where the EMIM density is greater than that of DCA. The orange color represents regions where DCA has a greater density than EMIM. (For interpretation of the references to color in this figure legend, the reader is referred to the web version of this article.)

The fact that the KB integrals for EMIM and DCA are positive indicates effective accumulation of the IL in the protein domain. As shown in Fig. 5B and 5D, the accumulation varies depending on the protein folding state. The KB integrals increase as the protein structure unfolds. Non-specific interactions between protein and ions (anion and cation peaks at 2.6 and 2.4 Å, respectively) are more common in systems with denatured and extended structures. The illustrative examples discussed above using systems with ensembles of native and denatured structures in 1.5 mol/L EMIMDCA solutions suggest that the observed increase in preferential solvation of more unfolded states is primarily due to interactions with neutral residues (which are more exposed to solvents in unfolded conformations), as shown in Fig. 8A and 8B.

3.3. Effect of the ion exchange in Ubiquitin-IL interactions

The distribution of the counterions is influenced by the exchange of the accompanying cation or anion, as previously demonstrated [18]. Non-specific interactions with polar and aliphatic residues lead to a greater BMIM accumulation at 2.4 Å than EMIM. DCA, on the other hand, exhibits a higher density in the protein's proximity than BF4 with the same cation. This section will explore some aspects of cation and anion exchanges on protein solvation structure.

MDDFs and KB integrals of EMIM and BF4 in systems in 1.5 mol/L EMIMBF4 solutions are shown in Fig. 9. Similar to DCA (Fig. 5A), BF4 MDDFs have two distinct accumulation steps (Fig. 9A). The first peak, at ∼1.9 Å, is due to polar bonds between fluorine atoms and protein surface atoms, while the second peak, at ∼2.6 Å, is related to non-specific interactions. The relative height of the BF4 MDDF peaks (Fig. 9A) is lower than that of the DCA MDDFs for all structure sets (Fig. 5A). For instance, in the system with native conformation, the first peak of BF4 MDDF is approximately 2.5 times smaller than for DCA, something expected from the fact that fluor is not a strong hydrogen bond acceptor.

Fig. 9A and B display the MDDFs and KB integrals for BF4 in EMIMBF4 solutions. EMIM participates mostly in non-specific interaction with the protein surface, as shown by the notable peaks of the MDDFs at ∼2.6 Å. Negative KB integrals for BF4 relative to the native and perturbed structure sets indicate that the anion is excluded from the protein domain. The BF4 KB integral relative to the denatured structure set, in turn, is close to zero. This means that the accumulation that occurs far from the protein surface is only enough to compensate for the initial exclusion associated with the protein and solute volumes. For both ions, EMIM and BF4, only the KB integral relative to the extended structure is positive. The greater KB integrals are observed, in all cases, for the most denatured protein conformations. Although the general behavior concerning the KB integrals is the same, the extent to which accumulation in the protein domain occurs is different. For instance, the KB integral in the system with the extended conformation for DCA is ∼55 L mol^{-1} while that for BF4 is ∼8 L mol^{-1}, about 6.8 times greater. Thus, the effective accumulation of BF4 ions in the protein domain is much smaller than that of DCA.

Table 3 shows the number of hydrogen bonds (as defined by the default geometric parameters in VMD) between the anions and the protein in systems with 1.5 mol/L IL solution. One can note that the number of hydrogen bonds formed between DCA and protein is greater than that formed between BF4 and protein for all conformation sets. It is noteworthy that the number of hydrogen bonds with the extended conformations is greater than with the other sets. In comparison to the native conformation, the extended conformation effectively eliminates protein-protein hydrogen bonds, particularly those of the main chain. As shown in tables S4, S5, and S6 in the supplementary material, hydrogen bonds that used to occur in protein bonds now occur with IL anions and water.

Fig. 10 shows the effect of changing the anion from DCA to BF4 on EMIM MDDFs and KB integrals in systems with 1.5 mol/L IL solutions. EMIM MDDFs have the same shape independently of the anion (Fig. 10A) or protein conformation (compare Fig. 10A and 10B). However, as shown in Fig. 10A and 10B, the height of the peak at ∼2.4 Å for EMIM with DCA is greater than EMIM with

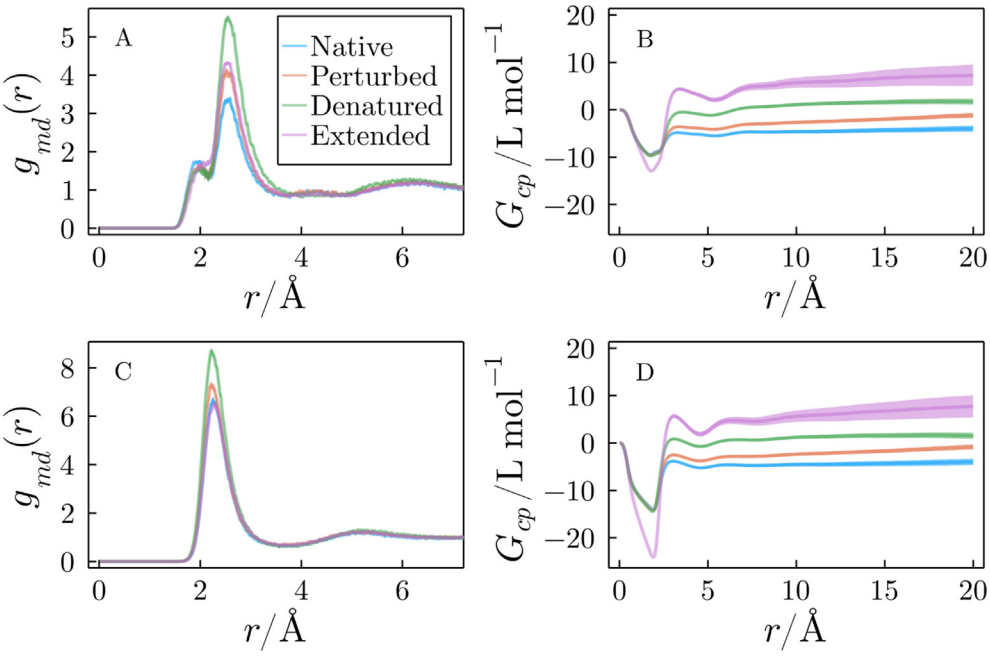

Fig. 9. (A) MDDFs and (B) KB integrals for BF4 relative to Ubiquitin in different conformational states in solutions of ∼1.5 mol/L EMIMBF4. (C) MDDFs and (D) KB integrals for EMIM in the same solution. In (A) and (C), we observe that BF4 MDDFs follow a similar pattern to MDDFs in the EMIMDCA solution. (B) and (D) suggest a progressive accumulation of EMIM and BF4 in the domain of more unfolded structures.

Table 3
Number of hydrogen bonds between DCA or BF4 and Ubiquitin. The hydrogen bonds were calculated in systems with 1.5 mol/L of the ionic liquids EMIMDCA and EMIMBF4, assuming only a geometric criterion for classification. The data is available for the native, perturbed, denatured, and extended conformations. For all systems, DCA establishes more hydrogen bonds than BF4. The fluctuations come from the calculation for 20 different simulations for each system.

Unfolding state	Number of hydrogen bonds DCA - Protein (1.5 mol/L)	Number of hydrogen bonds BF4 - Protein (1.5 mol/L)
Native	11.4 ± 0.2	5.10 ± 0.02
Perturbed	9.7 ± 0.2	4.87 ± 0.03
Denatured	11.0 ± 0.3	5.29 ± 0.03
Extended	20.82 ± 0.05	11.30 ± 0.01

BF4. Furthermore, EMIM density with DCA is 8.5 times greater than bulk at ∼2.4 Å from the native protein surface (Fig. 10A), and 12 times greater than bulk near denatured structures (Fig. 10B). The KB integrals reveal two major points: the first is that EMIM accumulates more when the system contains DCA, and the second is that EMIM accumulation in the protein domain is greater in a system for structure with greater surface area.

Thus, as depicted in Fig. 10, DCA promotes an increase in the concentration of EMIM near the protein (Supplementary Fig. S34 displays a map distribution of EMIM with DCA and EMIM with BF4 similar to Fig. 8). The presence of DCA, an anion that forms stronger contacts with the surface of proteins, clearly promotes the concentration of EMIM in protein proximal regions. As illustrated in Fig. 8, the concentration of IL is greater near neutral residues. For more open structures, non-specific interactions between protein and IL occur. The magnitude of these interactions, however, varies between DCA and BF4, leading to the greater concentration of EMIM around protein residues with DCA relative to BF4.

The cation type also affects the anion distribution. The presence of the BMIM cation makes the MDDFs and KB integrals increase, in fact, the DCA KB integrals for the system with BMIM are substantially greater than with EMIM for native and denatured conformation (Fig. S35). BMIM cation is larger and more hydrophobic than EMIM, thus nonspecific interactions between the protein and the cation increase. Because of the correlation between the distribution of the cation and the anion, the anion becomes more concentrated around the protein in the presence of the BMIM cation. As a result, when compared to the EMIM cation, the BMIM cation causes the DCA anion to be more effectively accumulated in the protein domains. Larger preferential solvation parameters are obtained, particularly for more unfolded structures, giving the BMIMDCA ionic liquid the strongest denaturing character among the IL solutions studied (Figs. S2 to S17).

3.4. Hydration of Ubiquitin in different folding states

Fig. 11A depicts the minimum-distance distribution functions (MDDFs) of water relative to Ubiquitin in ∼1.5 mol/L EMIMDCA solution, for each of the four structure sets. The first peak, at ∼1.8 Å, is characteristic of hydrogen bonds. It exhibits more than a twofold increase in water density above the reference state, for example, in the native conformations (blue).

The height of the peaks varies with Ubiquitin's conformational state. The first peak becomes less pronounced as the protein denatures. This is due to the increased protein surface area, which exposes residues that are less polar than those found on the native protein surface on average. For the perturbed, extended, and denatured conformations, the MDDF peak corresponding to hydrogen-bonding has maximum values of 1.7, 1.4, and 1.2, respectively. The peak at 2.5 Å, on the other hand, reflects the protein's second hydration shell and does not vary significantly among the different structure ensembles.

Table 4 displays the ratio between the number of hydrogen bonds (HB) between the protein and water in 1.5 mol/L EMIMDCA solutions. The average solvent-accessible surface area (SASA) of the conformations and the number of hydrogen bonds per surface area unit are also shown. There are more HBs for each unit of SASA in the native and least unfolded protein conformations. For instance,

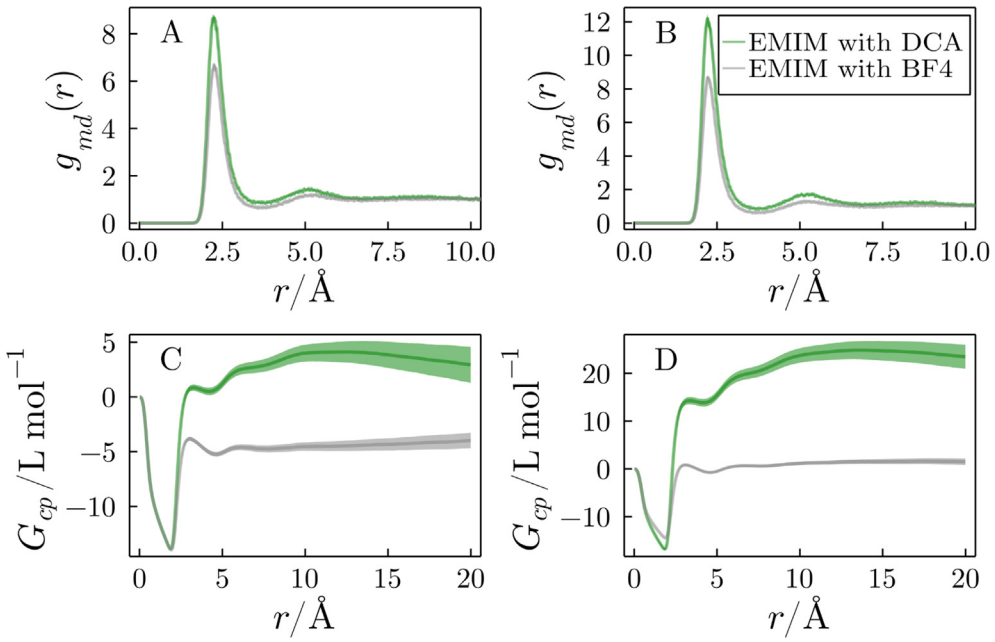

Fig. 10. MDDFs and KB integrals for EMIM in systems with native (A and C) and denatured (B and D) structures sets with 1.5 molL^{-1} EMIMDCA (green curve) and EMIMBF4 (gray curve) solutions. MDDFs show that DCA induces a greater increase of the EMIM concentration in the protein vicinities in comparison to BF4. (For interpretation of the references to color in this figure legend, the reader is referred to the web version of this article.)

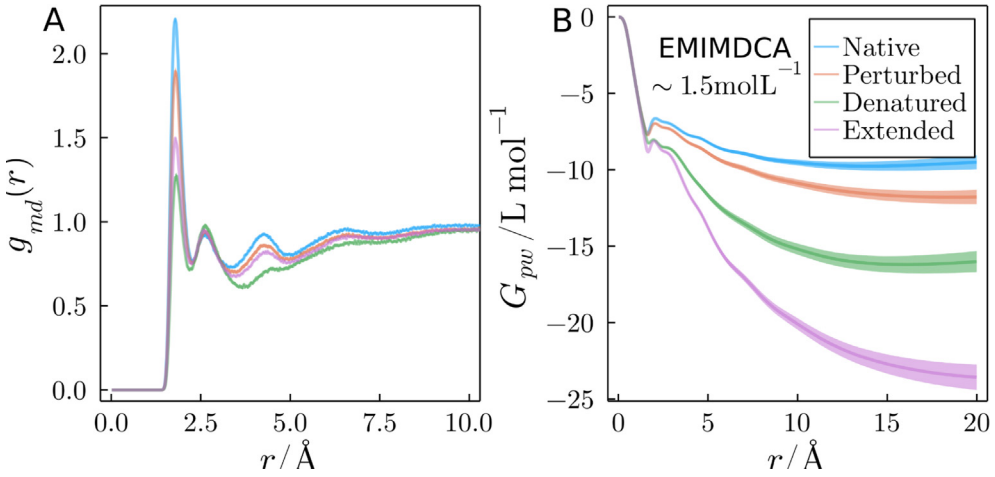

Fig. 11. (A) MDDFs and (B) KB integrals for water relative to Ubiquitin in different conformational states in solutions of ~1.5 mol/L EMIMDCA. In (A), we observe that water local density augmentation at hydrogen-bonding distances decreases as the protein undergoes denaturation, associated with an increased hydrophobic surface area. The effect of the greater hydrophobic surface is more notable in figure (B), which shows that when the protein core is exposed, water is progressively excluded from the protein domain. The colorful bands surrounding the solid lines are the standard errors calculated from 20 separate simulations.

Table 4
Number of hydrogen bonds between protein and water, protein-protein (intramolecular), and protein-anion. The data was calculated from systems with 1.5 mol/L EMIMDCA solutions. Additional data for all concentrations and ILs simulated in this work are available in Tables S4, S5, and S6 in the supplementary material.

Structure set	EMIMDCA				EMIMBF4			
	water	Protein-Protein	Protein -DCA	water HB / SASA	water HB	Protein-Protein	Protein - BF4	water HB / SASA
Native	140.2	56.9	11.4	2.8	150.9	5.38	5.1	3.0
Perturbed	124.8	59.7	9.7	2.4	135.5	59.3	4.9	2.6
Denatured	115.3	60.0	11.0	1.5	104.3	69.1	5.3	1.4
Extended	195.4	6.9	20.8	1.7	224.6	7.3	11.3	1.9

the number of HBs per unit area, respectively, 2.81 and 1.55 for the native and denatured models in EMIMDCA solutions. Therefore, water molecules interact relatively more through hydrogen bonds with the more folded protein structures set.

Fig. 11B shows the water KB integrals in 1.5 mol/L EMIMDCA solutions. The larger the protein surface area, the smaller the water KB integral. The establishment of hydrogen bonds in the initial solvation shell is insufficient to compensate for the excluded volumes

and water depletion over longer distances. As the structure diverges from the native form, therefore, the protein is dehydrated (MDDFs and KB integrals for all components in all systems simulated are available at the supplementary material from Figs. S2 to S17 and suggest the same trend).

Water, overall, is more excluded from the protein domain in systems with DCA systems than with BF4 (Figs. S2 to S17 in supplementary material). This is attributed to the stronger interaction between DCA and the protein. The number of hydrogen bonds (Table 4) between DCA and the protein support this picture The HB/SASA ratios for water in the EMIMBF4 solution are greater than those of water with EMIMDCA. Ultimately, the previous examples (1.5 mol/L EMIMDCA and EMIMBF4 solutions) demonstrate that water is less excluded from the protein domain of compact conformations. Figs. S2 to S17 and Tables S2 and S3 (included in the supplementary material) confirm these findings for the ILs BMIMDCA and BMIMBF4.

Our findings are consistent with those of previous studies. Diddens et al. [86], for example, used simulation to investigate the stability of a small peptide in various aqueous IL solutions. The authors demonstrated that EMIM dispersive interactions with the peptide favor a strong accumulation of cations around the native conformation of the peptide. The anions, in turn, interact with the EMIM shell via electrostatic interactions, compensating for the net positive charge of the EMIM shell. According to the authors, the size of the anions is the primary driving force for the denaturation mechanism by ILs. The establishment of favorable interactions between the cations and the anions causes an expansion of the solvent-accessible surface area, causing the peptide to denature with large anions (such as acetate). These results are complementary to our analysis because the main driving force for the increase in preferential IL solvation in the analysis of DCA and BF4 anions is the specific interactions between DCA/BF4 and the protein. In our case, DCA's much greater ability to form hydrogen bonds with the protein than BF4 causes the ILs containing DCA to solvate the protein much more strongly. Because the anions DCA and BF4 are similar in size, the main difference in the increase of IL accumulation in the protein domain must be specific interactions.

4. Conclusions

Here, we investigate Ubiquitin solvation in ionic liquid solutions as a function of the protein folding state. The ILs studied preferentially bind the native protein at lower concentrations, but happen to be preferentially excluded at some higher concentrations. This could suggest that these IL solutions could act as denaturants at lower concentrations, but stabilizers when concentrated. However, we show that the denatured forms of the protein interact more favorably with the IL ions because they expose a greater surface area with a greater abundance of non-polar and aliphatic residues. The cooperative behavior of the cation and anion of the ILs is deeply correlated with the denaturing strength of the solution: stronger direct ion-protein interactions promote the stabilization of both the hydrophilic exposed protein surface through hydrogen bonding with the IL anion, and of the hydrophobic residues through non-specific interactions with larger aliphatic cations. There is also cooperation between the exposure of the more hydrophobic protein core and the affinity of the IL to this surface, leading to further stabilization of the unfolded protein conformations.

CRediT authorship contribution statement

Vinicius Piccoli: Formal analysis. **Leandro Martínez:** Conceptualization, Formal analysis, Funding aquisition, Writing.

Data availability

Data will be made available on request.

Declaration of Competing Interest

The authors declare that they have no known competing financial interests or personal relationships that could have appeared to influence the work reported in this paper.

Acknowledgments

The authors acknowledge the financial support of Fapesp (2010/16947-9, 2018/24293-0, 2013/08293-7, 2018/14274-9, 2020/04916-3) and CNPq (302332/2016-2). Research developed with the help of CENAPAD-SP (National Center for High Performance Processing in São Paulo), project UNICAMP / FINEP - MCTI. This study was financed in part by the Coordenação de Aperfeiçoamento de Pessoal de Nível Superior - Brasil (CAPES) - Finance Code 001. The authors also thank the suggestions of two anonymous referees that improved the quality of the paper.

Appendix A. Supplementary material

Supplementary data to this article can be found online at https://doi.org/10.1016/j.molliq.2022.119953.

References

[1] T. Welton, Room-Temperature Ionic Liquids. Solvents for Synthesis and Catalysis, Chem. Rev. 99 (8) (1999) 2071–2084.
[2] J.P. Hallett, T. Welton, Room-temperature ionic liquids: solvents for synthesis and catalysis. 2, Chem. Rev. 111 (2011) 3508–3576.
[3] A. Schindl, M.L. Hagen, S. Muzammal, H.A.D. Gunasekera, A.K. Croft, Proteins in Ionic Liquids: Reactions, Applications, and Futures, Front Chem. 7 (2019) 347.
[4] R. Patel, M. Kumari, A.B. Khan, Recent advances in the applications of ionic liquids in protein stability and activity: a review, Appl. Biochem. Biotechnol. 172 (8) (2014) 3701–3720.
[5] M. Freemantle, Designer Solvents, Chem. Eng. News Archive. 76 (13) (1998) 32–37.
[6] R.D. Rogers, K.R. Seddon, Chemistry. Ionic liquids–solvents of the future?, Science 302 (5646) (2003) 792–793
[7] A. Pinkert, K.N. Marsh, S. Pang, M.P. Staiger, Ionic liquids and their interaction with cellulose, Chem. Rev. 109 (12) (2009) 6712–6728.
[8] V.I. Pârvulescu, C. Hardacre, Catalysis in ionic liquids, Chem. Rev. 107 (6) (2007) 2615–2665.
[9] J.L. Anderson, D.W. Armstrong, Immobilized ionic liquids as high-selectivity/high-temperature/high-stability gas chromatography stationary phases, Anal. Chem. 77 (19) (2005) 6453–6462.
[10] J. Muzart, Ionic liquids as solvents for catalyzed oxidations of organic compounds, Adv. Synth. Catal. 348 (3) (2006) 275–295.
[11] A.E. Visser, R.P. Swatloski, S.T. Griffin, D.H. Hartman, R.D. Rogers, Liquid/liquid extraction of metal ions in room temperature ionic liquids, Sep. Sci. Technol. 36 (5-6) (2001) 785–804.
[12] C. Schröder, Proteins in Ionic Liquids: Current Status of Experiments and Simulations, Top. Curr. Chem. 375 (2017) 25.
[13] A. Kumar, P. Venkatesu, Innovative aspects of protein stability in ionic liquid mixtures, Biophys. Rev. 10 (3) (2018) 841–846.
[14] D.T. Dang, S.H. Ha, S.-M. Lee, W.-J. Chang, Y.-M. Koo, Enhanced activity and stability of ionic liquid-pretreated lipase, J. Mol. Catal. B Enzym. 45 (3-4) (2007) 118–121.
[15] A.Y. Patel, K.S. Jonnalagadda, N. Paradis, T.D. Vaden, C. Wu, G.A. Caputo, Effects of Ionic Liquids on Metalloproteins, Molecules 26 (2) (2021) 514.
[16] C. Lange, G. Patil, R. Rudolph, Ionic liquids as refolding additives: N'-alkyl and N'-(omega-hydroxyalkyl) N-methylimidazolium chlorides, Protein Sci. 14 (2005) 2693–2701.
[17] M. Reslan, V. Kayser, Ionic liquids as biocompatible stabilizers of proteins, Biophys. Rev. 10 (3) (2018) 781–793.
[18] J. Smiatek, Aqueous ionic liquids and their effects on protein structures: an overview on recent theoretical and experimental results, J. Phys. Condens. Matter. 29 (2017) 233001.
[19] H.-J. Tung, J. Pfaendtner, Kinetics and mechanism of ionic-liquid induced protein unfolding: application to the model protein HP35, Mol. Syst. Des. Eng. 1 (2016) 382–390.
[20] P.L. Privalov, Cold denaturation of proteins, Crit. Rev. Biochem. Mol. Biol. 25 (4) (1990) 281–306.

[21] S.N. Timasheff, The control of protein stability and association by weak interactions with water: how do solvents affect these processes?, Annu Rev. Biophys. Biomol. Struct. 22 (1) (1993) 67–97.
[22] K.D. Collins, Ions from the Hofmeister series and osmolytes: effects on proteins in solution and in the crystallization process, Methods 34 (2004) 300–311.
[23] E.J. Guinn, L.M. Pegram, M.W. Capp, M.N. Pollock, M.T. Record, Quantifying why urea is a protein denaturant, whereas glycine betaine is a protein stabilizer, Proc. Natl. Acad. Sci. USA 108 (41) (2011) 16932–16937.
[24] Y. Levartovsky, A. Shemesh, R. Asor, U. Raviv, Effect of Weakly Interacting Cosolutes on Lysozyme Conformations, ACS Omega 3 (11) (2018) 16246–16252.
[25] M.C. Stumpe, H. Grubmüller, Interaction of urea with amino acids: implications for urea-induced protein denaturation, J. Am. Chem. Soc. 129 (2007) 16126–16131.
[26] J.L. Cleland, D.I. Wang, Cosolvent assisted protein refolding, Biotechnology 8 (1990) 1274–1278.
[27] D.R. Canchi, A.E. García, Cosolvent effects on protein stability, Annu. Rev. Phys. Chem. 64 (1) (2013) 273–293.
[28] H. Herberhold, C.A. Royer, R. Winter, Effects of chaotropic and kosmotropic cosolvents on the pressure-induced unfolding and denaturation of proteins: an FT-IR study on staphylococcal nuclease, Biochemistry 43 (2004) 3336–3345.
[29] D.R. Canchi, D. Paschek, A.E. García, Equilibrium study of protein denaturation by urea, J. Am. Chem. Soc. 132 (7) (2010) 2338–2344.
[30] E.P. O'Brien, R.I. Dima, B. Brooks, D. Thirumalai, Interactions between hydrophobic and ionic solutes in aqueous guanidinium chloride and urea solutions: lessons for protein denaturation mechanism, J. Am. Chem. Soc. 129 (2007) 7346–7353.
[31] B. Hribar, N.T. Southall, V. Vlachy, K.A. Dill, How Ions Affect the Structure of Water, J. Am. Chem. Soc. 124 (41) (2002) 12302–12311.
[32] X. Chen, T. Yang, S. Kataoka, P.S. Cremer, Specific ion effects on interfacial water structure near macromolecules, J. Am. Chem. Soc. 129 (40) (2007) 12272–12279.
[33] L.M. Pegram, M.T. Record Jr, Hofmeister salt effects on surface tension arise from partitioning of anions and cations between bulk water and the air-water interface, J. Phys. Chem. B. 111 (2007) 5411–5417.
[34] J.L. England, G. Haran, Role of solvation effects in protein denaturation: from thermodynamics to single molecules and back, Annu. Rev. Phys. Chem. 62 (2011) 257–277.
[35] F. Hofmeister, Zur Lehre von der Wirkung der Salze, Naunyn. Schmiedebergs, Arch. Pharmacol. 24 (4-5) (1888) 247–260.
[36] B. Kang, H. Tang, Z. Zhao, S. Song, Hofmeister Series: Insights of Ion Specificity from Amphiphilic Assembly and Interface Property, ACS Omega 5 (2020) 6229–6239.
[37] T. Janc, M. Lukšič, V. Vlachy, B. Rigaud, A.-L. Rollet, J.-P. Korb, G. Mériguet, N. Malikova, Ion-specificity and surface water dynamics in protein solutions, Phys. Chem. Chem. Phys. 20 (48) (2018) 30340–30350.
[38] N. Galamba, Mapping structural perturbations of water in ionic solutions, J. Phys. Chem. B. 116 (17) (2012) 5242–5250.
[39] B.A. Deyerle, Y. Zhang, Effects of Hofmeister anions on the aggregation behavior of PEO-PPO-PEO triblock copolymers, Langmuir 27 (15) (2011) 9203–9210.
[40] Y. Zhang, P.S. Cremer, Chemistry of Hofmeister anions and osmolytes, Annu. Rev. Phys. Chem. 61 (1) (2010) 63–83.
[41] D.F. Parsons, M. Boström, P. Lo Nostro, B.W. Ninham, Hofmeister effects: interplay of hydration, nonelectrostatic potentials, and ion size, Phys. Chem. Chem. Phys. 13 (2011) 12352–12367.
[42] A. Kumar, P. Venkatesu, Does the stability of proteins in ionic liquids obey the Hofmeister series?, Int J. Biol. Macromol. 63 (2014) 244–253.
[43] H. Zhao, Effect of ions and other compatible solutes on enzyme activity, and its implication for biocatalysis using ionic liquids, J. Mol. Catal. B Enzym. 37 (1-6) (2005) 16–25.
[44] M. Persson, U.T. Bornscheuer, Increased stability of an esterase from Bacillus stearothermophilus in ionic liquids as compared to organic solvents, J. Mol. Catal. B Enzym. 22 (1-2) (2003) 21–27.
[45] N. Kaftzik, P. Wasserscheid, U. Kragl, Use of ionic liquids to increase the yield and enzyme stability in the β-galactosidase catalysed synthesis of N-acetyllactosamine, Org. Process Res. Dev. 6 (4) (2002) 553–557.
[46] P. Lozano, T. de Diego, J.P. Guegan, M. Vaultier, J.L. Iborra, Stabilization of alpha-chymotrypsin by ionic liquids in transesterification reactions, Biotechnol. Bioeng. 75 (2001) 563–569.
[47] V. Piccoli, L. Martínez, Correlated counterion effects on the solvation of proteins by ionic liquids, J. Mol. Liq. 320 (2020) 114347.
[48] L. Martínez, S. Shimizu, Molecular Interpretation of Preferential Interactions in Protein Solvation: A Solvent-Shell Perspective by Means of Minimum-Distance Distribution Functions, J. Chem. Theory Comput. 13 (2017) 6358–6372.
[49] L. Martínez, ComplexMixtures.jl: Investigating the structure of solutions of complex-shaped molecules from a solvent-shell perspective, J. Mol. Liq. 347 (2022) 117945, doi: 10.1016/j.molliq.2021.117945
[50] I.P. de Oliveira, L. Martínez, The shift in urea orientation at protein surfaces at low pH is compatible with a direct mechanism of protein denaturation, Phys. Chem. Chem. Phys. 22 (1) (2020) 354–367.
[51] A. Ben-Naim, in: Statistical thermodynamics for chemists and biochemists, Springer, New York, NY, 2013, https://doi.org/10.1007/978-1-4757-1598-9.
[52] E.A. Oprzeska-Zingrebe, J. Smiatek, Aqueous ionic liquids in comparison with standard co-solutes: Differences and common principles in their interaction with protein and DNA structures, Biophys. Rev. 10 (2018) 809–824.
[53] P. Ganguly, N.F.A. van der Vegt, Convergence of Sampling Kirkwood-Buff Integrals of Aqueous Solutions with Molecular Dynamics Simulations, J. Chem. Theory Comput. 9 (3) (2013) 1347–1355.
[54] V. Pierce, M. Kang, M. Aburi, S. Weerasinghe, P.E. Smith, Recent applications of Kirkwood-Buff theory to biological systems, Cell Biochem. Biophys. 50 (1) (2008) 1–22.
[55] I.L. Shulgin, E. Ruckenstein, A protein molecule in an aqueous mixed solvent: Fluctuation theory outlook, J. Chem. Phys. 123 (2005) 054909.
[56] I.L. Shulgin, E. Ruckenstein, A Protein Molecule in a Mixed Solvent: The Preferential Binding Parameter via the Kirkwood-Buff Theory, Biophys. J. 90 (2006) 704–707.
[57] D. Harries, J. Rösgen, A practical guide on how osmolytes modulate macromolecular properties, Methods Cell Biol. 84 (2008) 679–735.
[58] S. Weerasinghe, P.E. Smith, A Kirkwood−Buff Derived Force Field for Mixtures of Urea and Water, J. Phys. Chem. B. 107 (16) (2003) 3891–3898.
[59] P.E. Smith, Chemical potential derivatives and preferential interaction parameters in biological systems from Kirkwood-Buff theory, Biophys. J. 91 (3) (2006) 849–856.
[60] S. Shimizu, D.J. Smith, Preferential hydration and the exclusion of cosolvents from protein surfaces, J. Chem. Phys. 121 (2) (2004) 1148–1154.
[61] D.R. Canchi, P. Jayasimha, D.C. Rao, G.I. Makhatadze, A.E. Garcia, Molecular Mechanism for the Preferential Exclusion of Osmolytes from Protein Surfaces, Biophys. J. 104 (2013) 189a.
[62] S. Shimizu, Estimating hydration changes upon biomolecular reactions from osmotic stress, high pressure, and preferential hydration experiments, Proc. Natl. Acad. Sci. USA 101 (5) (2004) 1195–1199.
[63] Q. Zou, B.J. Bennion, V. Daggett, K.P. Murphy, The molecular mechanism of stabilization of proteins by TMAO and its ability to counteract the effects of urea, J. Am. Chem. Soc. 124 (7) (2002) 1192–1202.
[64] Y. Moskovitz, S. Srebnik, Conformational changes of globular proteins upon adsorption on a hydrophobic surface, Phys. Chem. Chem. Phys. 16 (23) (2014) 11698–11707.
[65] S. Vijay-Kumar, C.E. Bugg, W.J. Cook, Structure of ubiquitin refined at 1.8 angstroms resolution, J. Mol. Biol. 194 (1987) 531–544.
[66] D.V.D. Spoel, D. Van Der Spoel, E. Lindahl, B. Hess, G. Groenhof, A.E. Mark, H.J.C. Berendsen, GROMACS: Fast, flexible, and free, J. Comput. Chem. 26 (2005) 1701–1718.
[67] B. Kohnke, R. Thomas Ullmann, C. Kutzner, A. Beckmann, D. Haensel, I. Kabadshow, H. Dachsel, B. Hess, H. Grubmüller, A Flexible, GPU - Powered Fast Multipole Method for Realistic Biomolecular Simulations in Gromacs, Biophys. J. 112 (2017) 448a.
[68] L. Martínez, R. Andrade, E.G. Birgin, J.M. Martínez, PACKMOL: A package for building initial configurations for molecular dynamics simulations, J. Comput. Chem. 30 (2009) 2157–2164.
[69] J.M. Martínez, L. Martínez, Packing optimization for automated generation of complex system's initial configurations for molecular dynamics and docking, J. Comput. Chem. 24 (2003) 819–825.
[70] B. Doherty, X. Zhong, O. Acevedo, Virtual Site OPLS Force Field for Imidazolium-Based Ionic Liquids, J. Phys. Chem. B. 122 (11) (2018) 2962–2974.
[71] M.J. Robertson, J. Tirado-Rives, W.L. Jorgensen, Improved Peptide and Protein Torsional Energetics with the OPLS-AA Force Field, J. Chem. Theory Comput. 11 (7) (2015) 3499–3509.
[72] W.L. Jorgensen, J. Chandrasekhar, J.D. Madura, R.W. Impey, M.L. Klein, Comparison of simple potential functions for simulating liquid water, J. Chem. Phys. 79 (2) (1983) 926–935.
[73] T. Darden, D. York, L. Pedersen, Particle mesh Ewald: AnN·log(N) method for Ewald sums in large systems, J. Chem. Phys. 98 (1993) 10089–10092.
[74] G. Bussi, D. Donadio, M. Parrinello, Canonical sampling through velocity rescaling, J. Chem. Phys. 126 (2007) 014101.
[75] H.J.C. Berendsen, J.P.M. Postma, W.F. van Gunsteren, A. DiNola, J.R. Haak, Molecular dynamics with coupling to an external bath, J. Chem. Phys. 81 (8) (1984) 3684–3690.
[76] M. Parrinello, A. Rahman, Polymorphic transitions in single crystals: A new molecular dynamics method, J. Appl. Phys. 52 (1981) 7182–7190.
[77] M. Parrinello, A. Rahman, Strain fluctuations and elastic constants, J. Chem. Phys. 76 (5) (1982) 2662–2666.
[78] T. McSherry, A General Steepest Descent Algorithm, IEEE Trans. Aerosp. Electron. Syst. AES-12 (1) (1976) 12–22.
[79] J. Bezanson, A. Edelman, S. Karpinski, V.B. Shah, Julia: A Fresh Approach to Numerical Computing, SIAM Rev. 59 (2017) 65–98.
[80] B.M. Baynes, B.L. Trout, Proteins in Mixed Solvents: A Molecular-Level Perspective, J. Phys. Chem. B. 107 (2003) 14058–14067.
[81] P.E. Smith, Cosolvent Interactions with Biomolecules: Relating Computer Simulation Data to Experimental Thermodynamic Data, J. Phys. Chem. B 108 (2004) 18716–18724.
[82] W. Humphrey, A. Dalke, K. Schulten, VMD: Visual molecular dynamics, J. Mol. Graph. 14 (1996) 33–38.
[83] S.N. Timasheff, Protein-solvent preferential interactions, protein hydration, and the modulation of biochemical reactions by solvent components, Proc. Natl. Acad. Sci. USA 99 (15) (2002) 9721–9726.
[84] C.P. Woodbury Jr., Introduction to Macromolecular Binding Equilibria, CRC Press, Boca Raton, FL, 2007. https://doi.org/10.1201/b12823.
[85] S. Ghosh, S. Parui, B. Jana, K. Bhattacharyya, Ionic liquid induced dehydration and domain closure in lysozyme: FCS and MD simulation, J. Chem. Phys. 143 (2015) 125103.

[86] D. Diddens, V. Lesch, A. Heuer, J. Smiatek, Aqueous ionic liquids and their influence on peptide conformations: denaturation and dehydration mechanisms, Phys. Chem. Chem. Phys. 19 (31) (2017) 20430–20440.

[87] V. Lesch, A. Heuer, V.A. Tatsis, C. Holm, J. Smiatek, Peptides in the presence of aqueous ionic liquids: tunable co-solutes as denaturants or protectants?, Phys Chem. Chem. Phys. 17 (2015) 26049–26053.